Carbon Dioxide Capture for Storage in Deep Geologic Formations – Results from the CO_2 Capture Project

Geologic Storage of Carbon Dioxide with Monitoring and Verification

Volume 2

Elsevier Internet Homepage – http://www.elsevier.com
Consult the Elsevier homepage for full catalogue information on all books, major reference works, journals, electronic products and services.

Elsevier Titles of Related Interest

AN END TO GLOBAL WARMING
L.O. Williams
ISBN: 0-08-044045-2, 2002

FUNDAMENTALS AND TECHNOLOGY OF COMBUSTION
F. El-Mahallawy, S. El-Din Habik
ISBN: 0-08-044106-8, 2002

GREENHOUSE GAS CONTROL TECHNOLOGIES: 6TH INTERNATIONAL CONFERENCE
John Gale, Yoichi Kaya
ISBN: 0-08-044276-5, 2003

MITIGATING CLIMATE CHANGE: FLEXIBILITY MECHANISMS
T. Jackson
ISBN: 0-08-044092-4, 2001

Related Journals:
Elsevier publishes a wide-ranging portfolio of high quality research journals, encompassing the energy policy, environmental, and renewable energy fields. A sample journal issue is available online by visiting the Elsevier web site (details at the top of this page). Leading titles include:

Energy Policy
Renewable Energy
Energy Conversion and Management
Biomass & Bioenergy
Environmental Science & Policy
Global and Planetary Change
Atmospheric Environment
Chemosphere – Global Change Science
Fuel, Combustion & Flame
Fuel Processing Technology

All journals are available online via ScienceDirect: www.sciencedirect.com

To Contact the Publisher
Elsevier welcomes enquiries concerning publishing proposals: books, journal special issues, conference proceedings, etc. All formats and media can be considered. Should you have a publishing proposal you wish to discuss, please contact, without obligation, the publisher responsible for Elsevier's Energy program:

Henri van Dorssen
Publisher
Elsevier Ltd
The Boulevard, Langford Lane
Kidlington, Oxford
OX5 1GB, UK

Phone: +44 1865 84 3682
Fax: +44 1865 84 3931
E.mail: h.dorssen@elsevier.com

General enquiries, including placing orders, should be directed to Elsevier's Regional Sales Offices – please access the Elsevier homepage for full contact details (homepage details at the top of this page).

Carbon Dioxide Capture for Storage in Deep Geologic Formations – Results from the CO_2 Capture Project

Geologic Storage of Carbon Dioxide with Monitoring and Verification

Edited by

Sally M. Benson
Lawrence Berkeley Laboratory
Berkeley, CA,USA

and Associate Editors

Curt Oldenburg[1], Mike Hoversten[1] and Scott Imbus[2]
[1]Lawrence Berkeley National Laboratory
Berkeley, CA, USA
[2]Chevron Texaco Energy Technology Company
Bellaive, TX, USA

Volume 2

ELSEVIER
2005

Amsterdam – Boston – Heidelberg – London – New York – Oxford
Paris – San Diego – San Francisco – Singapore – Sydney – Tokyo

ELSEVIER B.V.
Radarweg 29
P.O. Box 211, 1000 AE Amsterdam
The Netherlands

ELSEVIER Inc.
525 B Street, Suite 1900
San Diego, CA 92101-4495
USA

ELSEVIER Ltd
The Boulevard, Langford Lane
Kidlington, Oxford OX5 1GB
UK

ELSEVIER Ltd
84 Theobalds Road
London WC1X 8RR
UK

First edition 2005

Library of Congress Cataloging in Publication Data
A catalog record is available from the Library of Congress.

British Library Cataloguing in Publication Data
A catalogue record is available from the British Library.

ISBN: 0-08-044570-5 (2 volume set)

Volume 1: Chapters 8, 9, 13, 14, 16, 17, 18, 24 and 32 were written with support of the U.S. Department of Energy under Contract No. DE-FC26-01NT41145. The Government reserves for itself and others acting on its behalf a royalty-free, non-exclusive, irrevocable, worldwide license for Governmental purposes to publish, distribute, translate, duplicate, exhibit and perform these copyrighted papers. EU co-funded work appears in chapters 19, 20, 21, 22, 23, 33, 34, 35, 36 and 37. Norwegian Research Council (Klimatek) co-funded work appears in chapters 1, 5, 7, 10, 12, 15 and 32.

Volume 2: The Storage Preface, Storage Integrity Preface, Monitoring and Verification Preface, Risk Assessment Preface and Chapters 1, 4, 6, 8, 13, 17, 18, 19, 20, 21, 22, 23, 24, 25, 26, 27, 28, 29, 30, 31, 32, 33 were written with support of the U.S. Department of Energy under Contract No. DE-FC26-01NT41145. The Government reserves for itself and others acting on its behalf a royalty-free, non-exclusive, irrevocable, worldwide license for Governmental purposes to publish, distribute, translate, duplicate, exhibit and perform these copyrighted papers. Norwegian Research Council (Klimatek) co-funded work appears in chapters 9, 15 and 16.

♾ The paper used in this publication meets the requirements of ANSI/NISO Z39.48-1992 (Permanence of Paper).
Printed in The Netherlands.

Carbon Dioxide Capture for Storage in Deep Geologic Formations, Volume 2
D.C. Thomas and S.M. Benson (Eds.)

Chapter 10

LEAKAGE OF CO_2 THROUGH ABANDONED WELLS: ROLE OF CORROSION OF CEMENT

George W. Scherer[1], Michael A. Celia[1], Jean-Hervé Prévost[1], Stefan Bachu[2], Robert Bruant[1], Andrew Duguid[1], Richard Fuller[1], Sarah E. Gasda[1], Mileva Radonjic[1] and Wilasa Vichit-Vadakan[3]

[1]Department of Civil & Environmental Engineering, Eng. Quad. E-319, Princeton University, Princeton, NJ 08544, USA
[2]Alberta Geological Survey, Alberta Energy and Utilities Board, Edmonton, AB, T6B 2X3, Canada
[3]Department Civil Engineering and Geological Science, University of Notre Dame, 160 Fitzpatrick Hall, Notre Dame, IN 46556, USA

ABSTRACT

The potential leakage of CO_2 from a geological storage site through existing wells represents a major concern. An analysis of well distribution in the Viking Formation in the Alberta basin, a mature sedimentary basin representative of North American basins, shows that a CO_2 plume and/or acidified brine may encounter up to several hundred wells. A review of the literature indicates that cement is not resistant to attack by acid, but little work has been reported for temperatures and pressures comparable to storage conditions. Therefore, an experimental program has been undertaken to determine the rate of corrosion and the changes in properties of oil well cements exposed to carbonated brine. Preliminary results indicate a very high rate of attack, so it is essential to have accurate models of the composition and pH of the brine, and the time that it will remain in contact with cement in abandoned wells. A model has been developed that incorporates a flash calculation of the phase distribution, along with analysis of the fluxes and pressures of the liquid, solid and vapor phases. A sample calculation indicates that wells surrounding the injection site may be in contact with the acidified brine for years.

INTRODUCTION

Possible leakage of injected CO_2, from the formation into which it is injected to other subsurface formations or to the atmosphere, constitutes a major concern associated with geological storage of captured CO_2 because it may contaminate existing energy, mineral and/or groundwater resources, pose a local hazard at the ground surface, and contribute to increased concentrations of CO_2 in the atmosphere. Possible pathways for leakage include diffuse leakage across cap rock formations, concentrated leakage through natural features such as faults and fractures, and leakage through human-made features such as wells. In areas where little exploration for, or production of, hydrocarbons has occurred, there are few existing wells, and potential leakage through them is not a major concern. (Although old exploration wells might leak, it would not be prohibitively expensive to repair a small number of wells.) However, in mature sedimentary basins, such as those found in North America, more than a century of exploration and production has resulted in a very large number of wells. For example, in the state of Texas in the United States, more than 1 million wells have been drilled [1], while in the Province of Alberta in Canada, more than 350,000 wells have been drilled, with approximately 15,000 new wells currently being drilled annually (www.eub.gov.ab.ca). A significant fraction of these wells are abandoned [2], and information about abandonment practices and general record keeping are of variable quality, especially for older wells. Because of the large number of wells in locations such as these, the potential for leakage through existing wells is an important concern that requires quantitative investigation. For context, a schematic of a possible well-leakage scenario is shown in Figure 1, where an injected CO_2 plume moves under

the influence of both pressure drive and buoyancy, and then some of the injected CO_2 moves vertically upward upon encountering a preferential flow path that corresponds to an abandoned well. It is this kind of scenario that requires quantitative analysis.

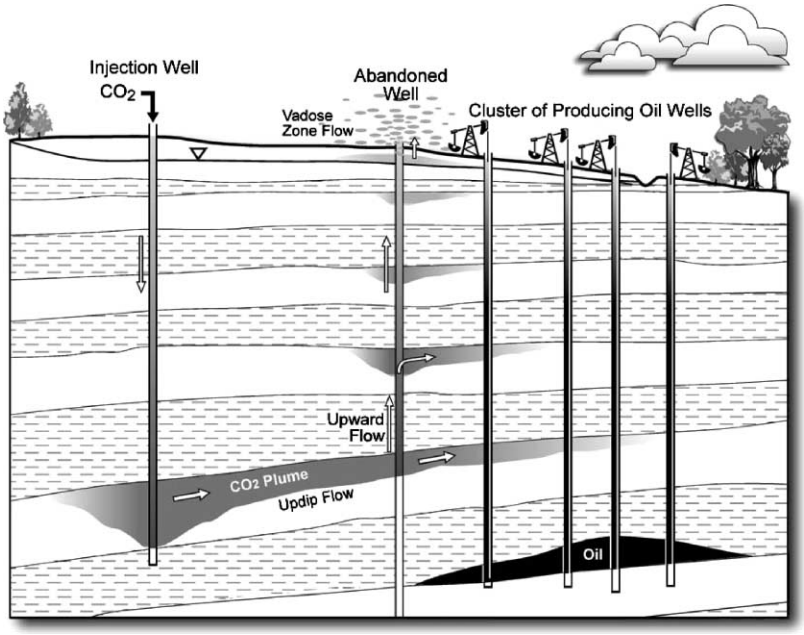

Figure 1: Schematic of injection site and leakage of CO_2 plume through an abandoned well that penetrates a formation in the sedimentary succession. From Ref. [2]. Reproduced with permission from Environmental Geology; copyright Springer, Berlin.

If an exploration well is drilled and the operator decides to abandon the well without further development, the open hole would typically be filled with a series of cement plugs. If the well is developed for production, then a casing would be inserted into the hole, and cement would be emplaced along a portion of the annular space between the casing and the rock. Possible leakage pathways along an existing well are shown schematically in Figure 2, and include preferential flow pathways along the rock–cement interface, the casing–cement interface, and through degraded materials. Because well-formed cement has very low permeability, of the order of 10^{-20} m^2 [3], no significant flow of CO_2 can occur unless there are preferential flow paths, or the material has degraded, or the material was not emplaced properly. If such preferential flows occur, then the overall well materials need to be assigned a quantitative measure of flow potential, which we might take to be the effective permeability of the composite materials associated with the well. Assignment of this composite measure requires estimation of cement degradation under in situ conditions, including possible contact with CO_2-rich fluids, some assessment of the initial emplacement of the cement, including its location along the well and the quality of the emplacement procedure, and knowledge of the location of wells in the vicinity of the injection operation. The first of these requires careful laboratory and modeling studies, which are the primary subject of this chapter, while the second and third require examination of historical records and detailed analysis of existing wells.

To place the problem in some context, consider a simple simulation in which one injection well and one possible leaky well are modeled, with injection and formation parameters as shown in Figure 3a. If we define the leakage fraction to be the rate of leakage along the leaky well (mass of CO_2 per time) divided by the CO_2 injection rate (mass of CO_2 per time), then the leakage fraction is a function of both the distance

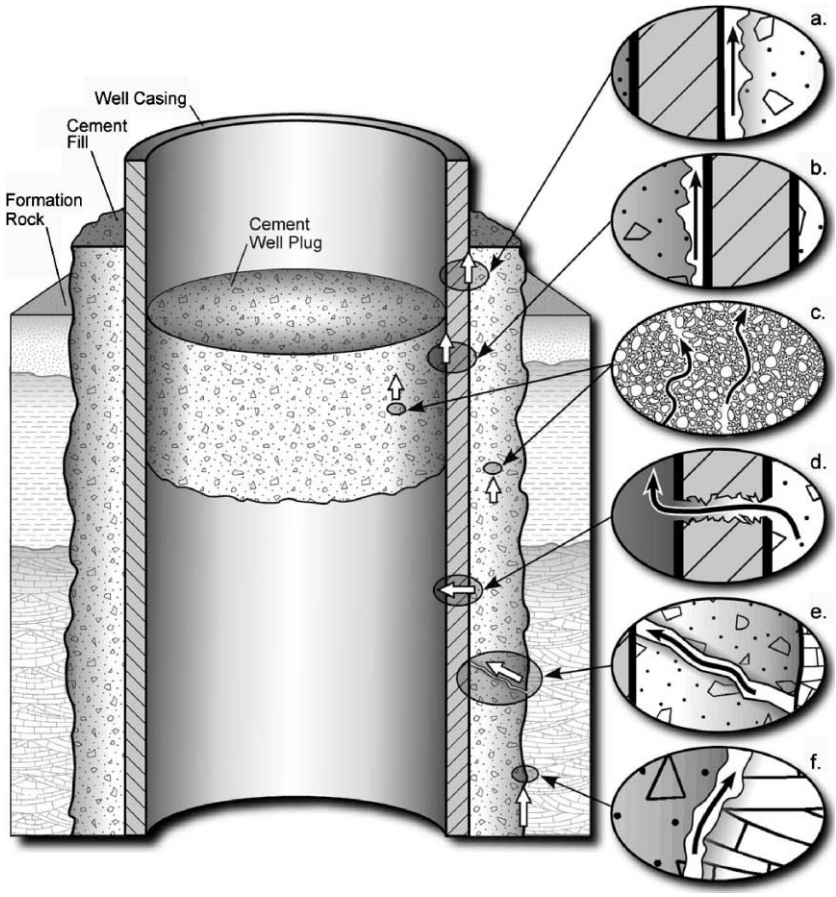

Figure 2: Schematic representation of possible leakage pathways through an abandoned well: (a) between casing and cement; (b) between cement plug and casing; (c) through the cement pore space as a result of cement degradation; (d) through casing as a result of corrosion; (e) through fractures in cement; and (f) between cement and rock. From Ref. [2]. Reproduced with permission from Environmental Geology; copyright Springer, Berlin.

between the two wells and the effective permeability of the leaky well. This relationship is captured in Figure 3b, which shows leakage fraction as a function of distance between the wells and abandoned-well permeability. This figure, taken from Ref. [4], shows that a very large increase in effective permeability is required to produce significant leakage: for a leakage fraction $> 1\%$ at a well spacing of 500 m, the effective permeability associated with the abandoned well must increase to about 10^{-10} m^2. This is many orders of magnitude larger than the permeability of intact cement, showing clearly that well-formed cement will not leak any CO_2. However, this value of effective permeability also corresponds to the effective permeability of an annular opening between the rock and cement that is 1 mm thick. So a thin (1 mm) degraded zone of cement, with very large permeability in the degraded zone, can lead to large effective permeabilities if the annular opening is continuous along the well. Therefore, while the material (cement) emplaced along the well has properties that can suppress all leakage, the system is also extremely sensitive to small irregularities in the system structure. Clearly this problem requires detailed studies of cements, on very small length scales, to properly capture possible small-scale system irregularities that can lead to significant

leakage rates. In addition, these detailed small-scale studies must ultimately couple to analyses of injection and leakage at the field scale. This very large range of length scales over which the leakage analysis must be performed, from millimeters to kilometers, is one of the features that makes this a challenging and scientifically interesting problem.

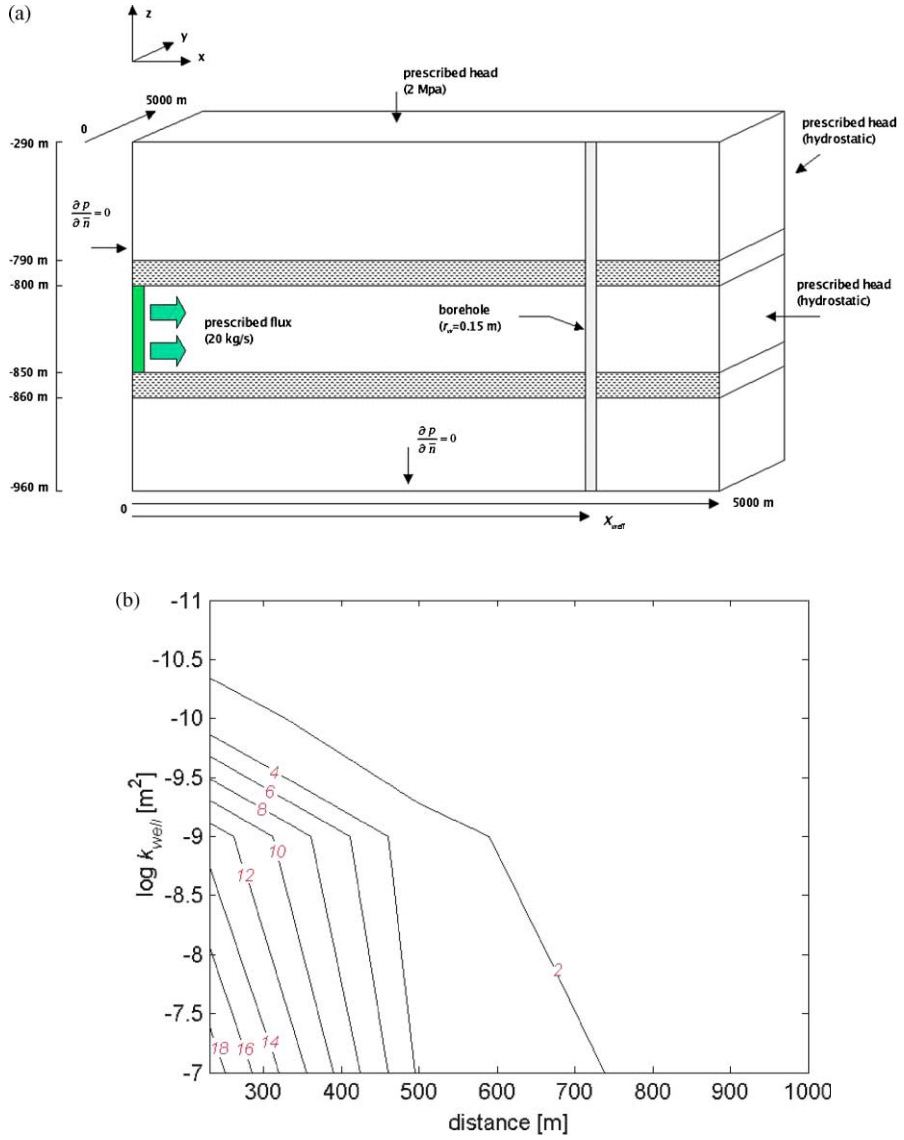

Figure 3: (a) Schematic of injection with leakage from a single passive well; (b) total leakage as a percentage of total CO_2 injected after 4 years at 20 kg/s in 2D parameter space. Leakage is a function of borehole location from injector well (x-axis) and the borehole effective permeability, k_{well} (y-axis). From Ref. [2].

Figure 3b provides the context for studying well leakage. If we can identify the values to be used on the two axes of the plot, we can estimate leakage along a well. Of course, the difficulty is in identification of these values along the axes. Consider first the distance. For some locations, all well locations are known and records are available; for others, this is not the case. In addition, we know that more than one well can be impacted by an injection operation. Therefore, in order to characterize the "distance" axis, we actually need to know many distances, associated with fields of existing wells. On the "permeability" axis, we need to have information about the well cements used, and we need to estimate degradation rates and the properties of degradation products. We then need a set of modeling tools that can integrate these data to produce meaningful estimates of leakage fractions associated with an individual injection operation or with a series of operations. Our research has focused on each of these three aspects of the well-leakage problem: spatial statistics of well locations in mature basins, cement degradation dynamics and small-scale geochemical modeling and large-scale modeling including many wells and uncertainties in their properties.

In this chapter, we review some of our work on spatial statistics of wells, and then present both experimental and modeling work related specifically to cement degradation. This work complements other ongoing work within our extended group that includes larger scale modeling of plume evolution and leakage [5–7], CO_2 transport through shallow unsaturated soils [8,9], geochemical responses and possible water quality changes in shallow aquifers due to introduction of leaked CO_2 [10], and analysis of plume evolution and extent in ongoing acid–gas injection operations [11].

SPATIAL ANALYSIS OF WELLS

Because the Alberta Basin has an outstanding database with a wide range of information on oil and gas wells, we conducted a study of well locations in a formation in Alberta in order to determine spatial characteristics of oil and gas well patterns in a mature basin. We analyzed all wells that penetrate the Viking Formation, which is an areally extensive formation that contains numerous oil and gas pools. Both a cross-section of the basin and the spatial location of all wells that penetrate the Viking Formation are shown in Figure 4. The well locations show clear clustering, which is expected given the nature of oil and gas pools in the formation and in the overall basin. In order to characterize the number of wells that one would expect to be impacted by an injection operation in the Viking Formation, we performed a cluster analysis and separated spatial regions into "high-density", "medium-density", and "low-density" areas. High-density areas, typically associated with oil production, constitute about 3% of the area while accounting for about 30% of the wells, and have mean well density of close to 4 wells per square kilometer. Medium-density wells account for another 30% of the wells, and have a density of about 1 well per square kilometer, and correspond roughly to gas-producing clusters. The low-density background wells cover close to 90% of the area, correspond to a bit more than one-third of the wells, and have a density of 0.15 wells per square kilometer. The low-density background regions also have the highest fraction of abandoned wells. Summary statistics are shown in Table 1.

These numbers can be translated into number of wells that would be impacted by a typical injection scenario. If we estimate a typical CO_2 plume to evolve radially on the order of 5 km, based on solutions in Lindeberg [12], Xu et al. [13] and others or Nordbotten et al. [5,6,14], then we can analyze the spatial data to determine the number of wells impacted by an injection. Results of such an analysis, taken from Gasda et al. [2], are shown in Figure 5, where for each of the three density classes we present a histogram based on a discretization of the data, showing how the number of wells varies for different points within clusters. We present these histograms for both the total number of wells (left column of three figures) and for only the abandoned wells within the specific density class (right column of figures). We see that in high-density areas, the number of wells impacted by a modest plume size of 5 km is several hundred; the mean is 240, and the largest value is greater than 700. For injections into the low-density background regions, the numbers are much more modest, with a mean of about 18 and a maximum number of 130; about 35% of the bins give an adjacent well count of zero. These numbers indicate that in the Viking Formation, injection operations should be expected to contact a significant number of existing wells, up to many hundreds per injection operation. Because the Viking Formation is characteristic of North America's onshore sedimentary basins, we expect these statistics to apply to other mature sedimentary basins.

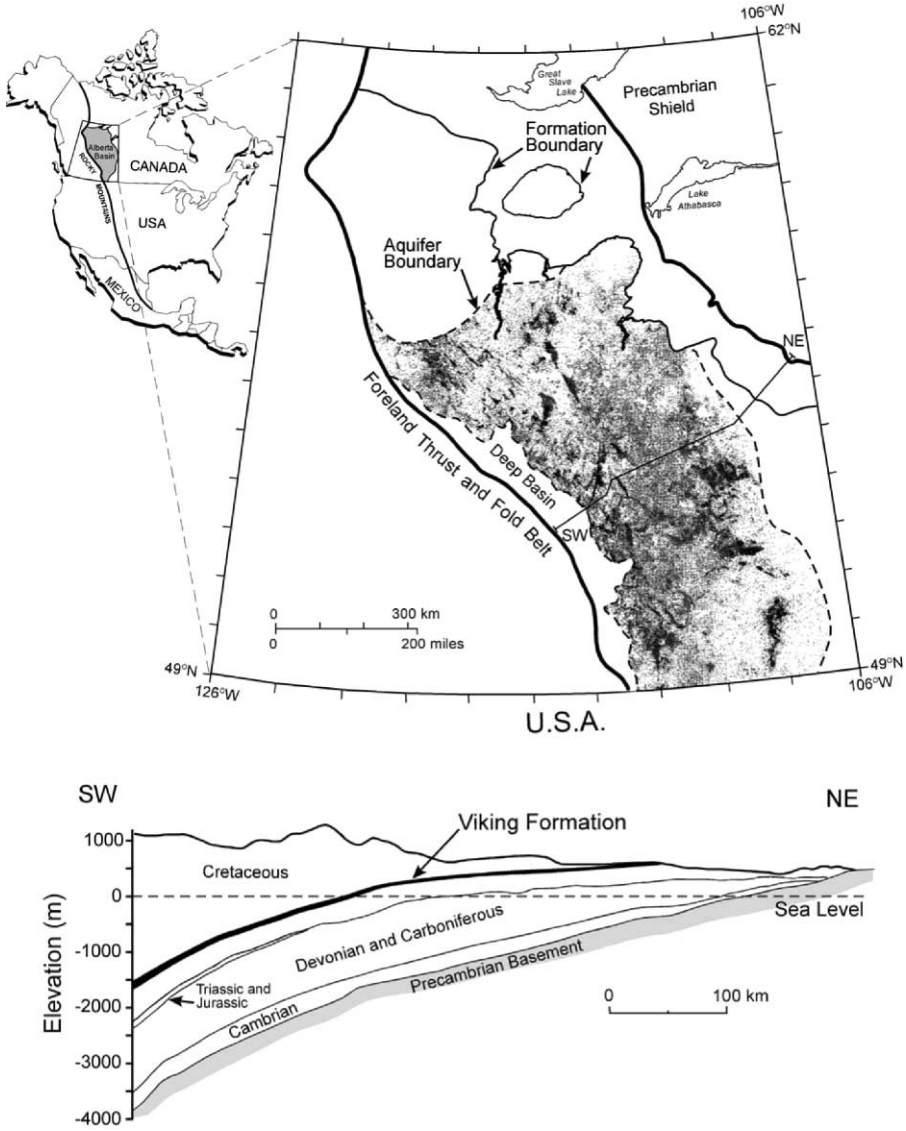

Figure 4: Location of the Viking aquifer in the Alberta basin, Canada: (a) plan view, showing also the location of all wells that penetrate the aquifer; (b) cross-section of the Alberta basin showing the location of the Viking Formation. From Ref. [2]. Reproduced with permission from Environmental Geology; copyright Springer, Berlin.

CEMENT DURABILITY

Cement is used to seal the annulus between the casing and the formation, as shown in Figure 2. Cement powder is mixed with water and various additives to control the density and rheology of the slurry,

TABLE 1
STATISTICS OF DISTRIBUTION OF WELLS IN THE VIKING AQUIFER OF THE ALBERTA BASIN

	High density	Medium density	Low density (background)
Number of clusters	268	963	–
Number of wells (% total)	28.0	28.6	38.2
Area (% total)	2.7	10	87.2
Mean intrinsic density (wells/km^2)	3.75	1.13	0.15
Fraction of wells abandoned (%)	28.9	45.0	50.0

pumped down through the casing and up the annulus. The rate of the hydration reaction must be carefully controlled, so that the cement paste does not harden prematurely. Once in place, the hardened cement paste must have strength, comparable to that of the surrounding formations, and low enough permeability to provide zonal isolation and to protect the steel casing [3]. Unfortunately, cement is not resistant to acids, so it will be attacked by the carbonated brines produced by storage of CO_2 in saline aquifers. Studies in the literature indicate that the rate of deterioration of the cement may be problematic, but there are no data specifically applicable to the range of temperature and pressure relevant for storage. In the following, we will briefly review the chemistry of cement and then summarize what is known about reaction of cement with carbon dioxide. Finally, we will describe a research program in our lab that is designed to provide quantitative information about the rate of reaction of cement under storage conditions, and the effect of the reaction on the relevant physical properties of the cement paste.

Cement Chemistry

In the following discussion we will use ordinary chemical notation, set in italics, and the shorthand notation commonly used in cement chemistry: $C = CaO$, $S = SiO_2$, $A = Al_2O_3$, $F = Fe_2O_3$, $H = H_2O$, $\bar{C} = CO_3$, and $\bar{S} = SO_4$. Thus, calcium hydroxide is represented as CH or $Ca(OH)_2$ and tricalcium aluminate as C_3A or $3CaO{\cdot}Al_2O_3$ or $Ca_3Al_2O_6$.

Ordinary Portland cement (OPC) is made by grinding calcium carbonate from a natural deposit of limestone, mixing it proportionally with clay, and firing the mixture in a rotary kiln at 1450 °C to form clinker [15]. Once clinker cools, it is ground to a mean particle size of approximately 30 μm. OPC is composed primarily of four compounds: C_3S, C_2S, C_3A, and C_4AF, which are defined in Table 2. The various types of cements shown in Table 3 differ in the ratios of the four compounds and in the fineness of the grind. Oil wells are generally made with Class G or H, which are very similar chemically to ASTM Type I (OPC), which is the most widely used cement in ordinary construction. Class H differs from Type I in that H has a larger particle size and its aluminate is primarily in the form of C_4AF, with little C_3A; both these factors increase the setting time of Class H relative to Type I.

The hydration of OPC at atmospheric temperature and pressure yields several products, but the one that is responsible for the strength of the hardened paste is colloidal calcium silicate hydrate (C-S-H), often called the "gel phase". C-S-H has no fixed composition (which is why the dashes are included in the abbreviation), but the average ratio of calcium to silicon is approximately 1.7 [16]. The building blocks are believed to be particles approximately 2.2 nm in diameter [17] having a semi-crystalline layered structure, with siloxane chains attached to sheets of Ca–O; variations in chain length and substitutions in the Ca–O sheets result in a range of stoichiometry and lattice spacing in the crystallites. Both C_2S and C_3S hydrate into C-S-H, but C_2S reacts much more slowly than C_3S, and C_3S produces three times as much CH as C_2S:

$$2C_3S + 6H \rightarrow C_3S_2H_3 + 3CH \quad (1)$$

$$2C_2S + 4H \rightarrow C_3S_2H_3 + CH \quad (2)$$

Figure 6 is an SEM picture of C-S-H with CH embedded. It is the CH that will play a significant role in the wet and dry carbonation processes. Although the amount of C_3A is small, it reacts violently with water and

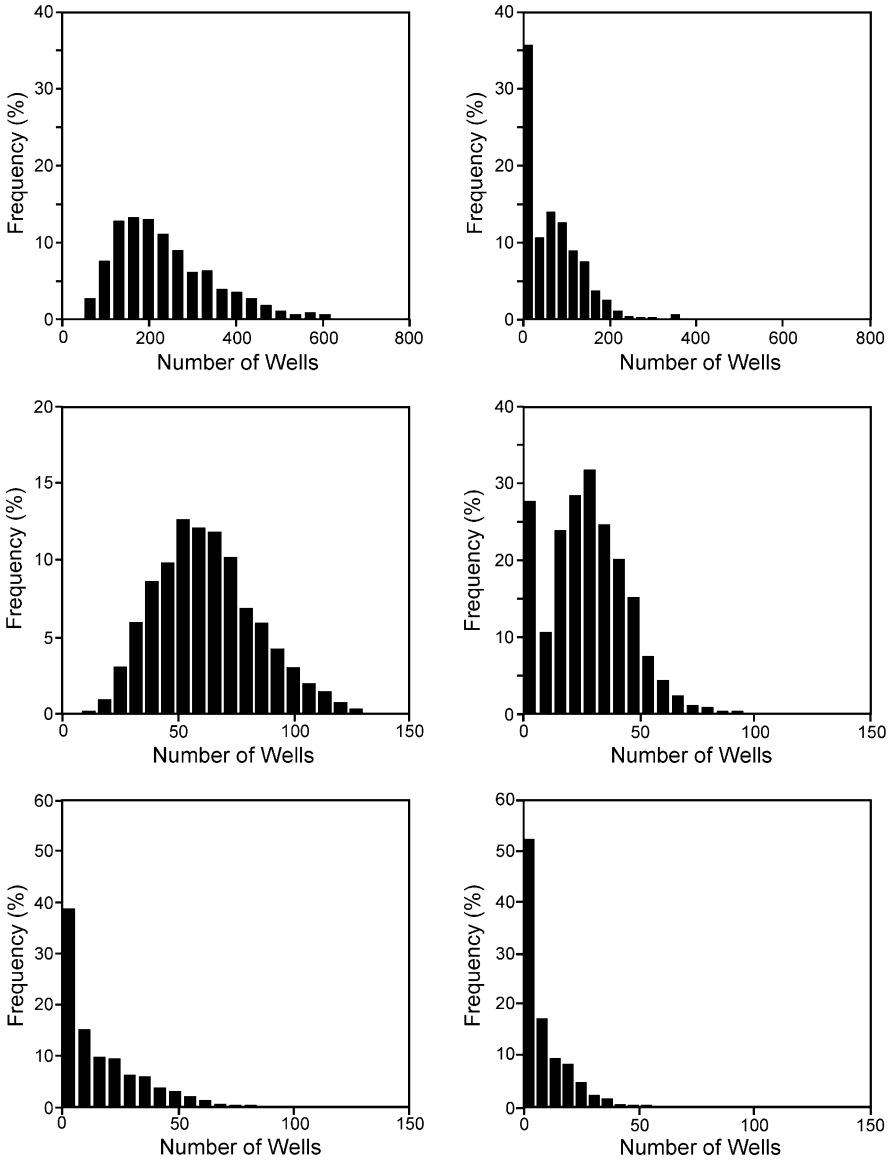

Figure 5: Frequency distributions for the number of wells within an approximate 5 km radius of a potential injection well—all wells in (a) high-density clusters, (b) medium-density clusters, (c) background;—and only abandoned wells in (d) high-density clusters, (e) medium-density clusters, (f) background. From Ref. [2]. Reproduced with permission from Environmental Geology; copyright Springer, Berlin.

TABLE 2
MAIN COMPOUNDS OF PORTLAND CEMENT [15]

Name of compound	Oxide composition	Abbreviation
Tricalcium silicate	$3CaO{\cdot}SiO_2$	C_3S
Dicalcium silicate	$2CaO{\cdot}SiO_2$	C_2S
Tricalcium aluminate	$3CaO{\cdot}Al_2O_3$	C_3A
Tetracalcium aluminoferrite	$4CaO{\cdot}Al_2O_3{\cdot}Fe_2O_3$	C_4AF

TABLE 3
TYPES AND CLASSES OF CEMENT

API class	ASTM type	C_3S (%)	C_2S (%)	C_3A (%)	C_4AF (%)
A	I	53	24	8 +	8
B	II	47	32	5 −	12
C	III	58	16	8	8
D		26	54	2	12
E		26	54	2	12
F		–	–	–	–
G		50	30	5	12
H		50	30	5	12

can create “flash set”, a sudden hardening of the mixture. This is avoided by the addition of gypsum, which converts aluminates to aluminosulfates, such as ettringite. The combination of the calcium silicate and aluminum hydrates and CH form the gel phase of hardened cement paste. The formation of a percolated gel phase is called “setting”, and it marks the transition from a fluid slurry to an elastic solid. The setting process is governed by C_3S and C_3A because these two have high rates of reaction. In contrast, C_2S governs the subsequent hardening process, which occurs over a period of weeks.

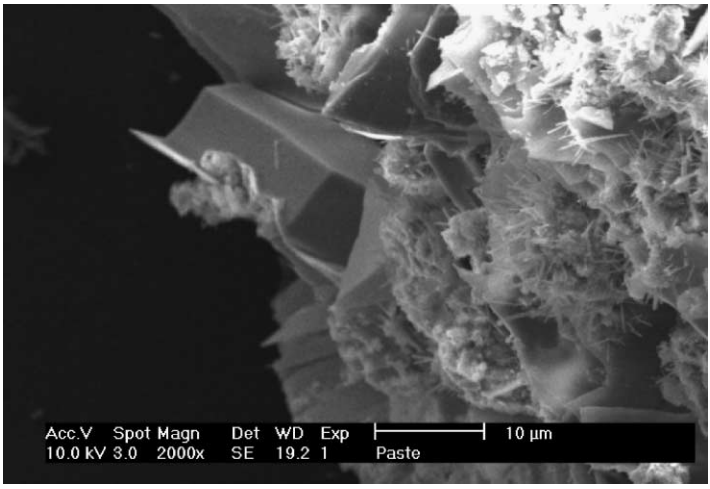

Figure 6: SEM photo showing large polyhedral crystals of CH embedded in C-S-H matrix.

At the setting point, the cement grains are lightly bonded by C-S-H, and the micron-scale interstices (called capillary pores) between the grains are filled with water. As the reaction proceeds, the water is consumed and the capillary pores are gradually filled with the gel phase, which has approximately 28% porosity and pores ranging from approximately 2 to 100 nm in diameter. The network of capillary pores initially controls the permeability of the paste, but the permeability drops drastically if the quantity of hydration products is sufficient to interrupt the capillary pores and force flow of pore liquid to pass through the gel. The pore structure is strongly affected by the particle size of the cement: the finer the grind, the smaller the interstices, and the easier they are to fill with hydration products. However, the most important factor is the water/cement ratio, w/c, used in hydration. If $w/c > 0.4$, then the volume of hydration products is not sufficient to fill the capillary pores; however, the capillary pore network can be blocked (depercolated) by gel at higher w/c. When the permeability is high, chemical attack on the hydrated paste can be very fast, because its surface area is quite high (approximately 50–300 m^2/g).

The exposure of hydrated cement to high temperature and pressure results in the transformation of the amorphous C-S-H gel into other crystalline forms, as shown in Figure 7. The transformation is gradual and depends on the temperature and pressure of the system. Xonotlite (C_6S_6H), a substantially weaker and more porous material than C-S-H, is commonly found in geothermal wells [16]. Silica-rich materials, called pozzolanic admixtures, prevent or delay the strength retrogression by reacting with CH to form more C-S-H. The delay in strength retrogression is partly due to an increased quantity of C-S-H for conversion. In addition, the presence of additional silica shifts the ratio of CaO/SiO_2 down, which can cause other crystal structures to form, as shown in Figure 7.

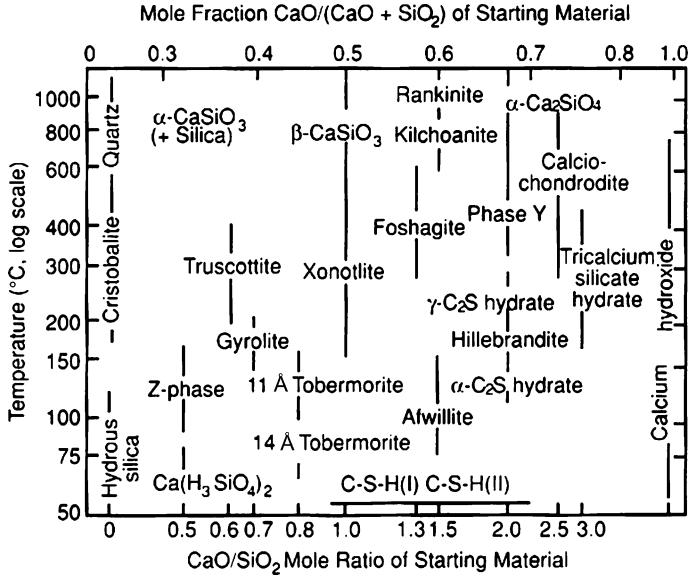

Figure 7: High-temperature phases of calcium silicate [3].

Reaction with CO_2

When moist OPC is exposed directly to dry CO_2, the calcium hydroxide is carbonated to form calcium carbonate ($CaCO_3$ or $C\bar{C}$):

$$Ca(OH)_2 + CO_2 \rightarrow CaCO_3 + H_2O \tag{3}$$

The increase in molar volume from 26.2 cm^3/mole for CH to 33.1 cm^3/mole for $C\bar{C}$ makes the cement stronger and less permeable [15]. The effect of carbonation on C-S-H is more complicated, as explained below.

Exposure to supercritical CO_2 has been shown to increase the strength and reduce the permeability of concrete [18], so exposure to dry CO_2 during injection is not expected to harm cement, However, when CO_2 is introduced into an aquifer, the chemistry changes drastically, because dissolution of CO_2 in water creates carbonic acid (H_2CO_3). Hydrated cement is a highly alkaline material that is chemically stable only when pH $>$ 10 [16]. Therefore, the introduction of large quantities of CO_2 into an aquifer will make the downhole conditions extremely aggressive against the existing cement.

The capacity for water to dissolve CO_2 increases with pressure and decreases with rising temperature. Therefore, the depth of storage will play a significant role in the capacity of the aquifer to hold CO_2, as indicated in Figure 8, which shows how the pH of the aquifer varies according to the depth of injection. In a quartzitic sandstone formation, the pH is about 3 over the range of depth of interest; even in equilibrium with limestone, the pH is about 5. Solutions with such low pH can attack cement rapidly.

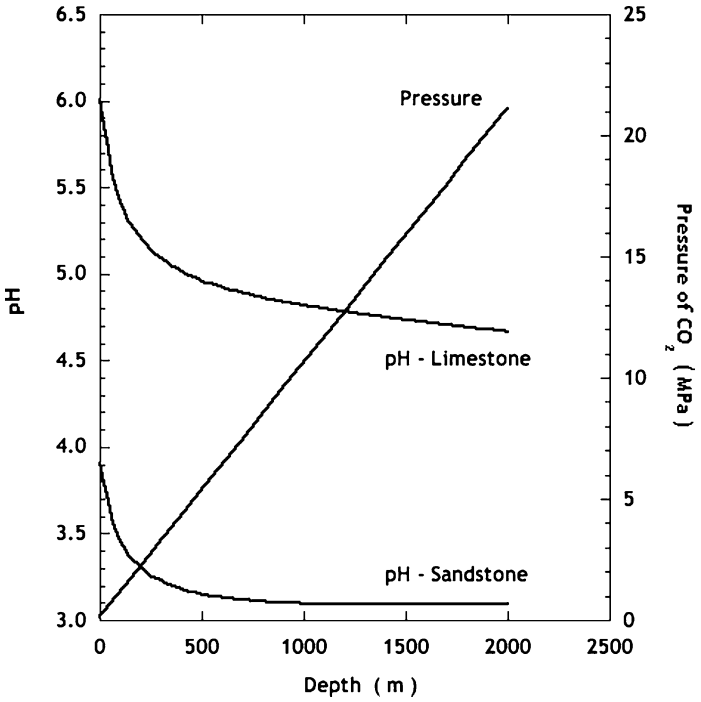

Figure 8: pH of a pure water aquifer upon equilibration with CO_2 at the formation temperature and pressure, calculated using EQ3/6 v. 7.2.

Calcium hydroxide is a product of cement hydration, as shown in Eqs. (1) and (2), and constitutes the alkaline reserve to provide acidic resistance [19]. Although the solubility of CH is quite low (approximately 1–2 g/kg of water), leaching of CH from cement by water has been well documented in the literature [20–26]. The consequences of the removal of CH include lower pH, higher porosity, higher permeability, and lower strength. A lower pH allows steel to corrode and oxidize, and the stability of the C-S-H gel is compromised when the pH drops below 10. Increased porosity and permeability allow greater influx of contaminants and aggressive agents, so the corrosion process accelerates.

Powers et al. [20] found that leaching of CH occurred during permeability measurement. Continuing hydration of the cement offsets the leaching effect during the first 600 days, but once the cement was fully

hydrated, the effect of leaching as indicated by the increasing permeability became obvious. More recently, Carde et al. [23] performed a series of experiments on pure OPC paste and paste with silica. They concluded that the macroporosity created through the leaching of CH leads to decreasing strength; since macroporosity controls transport properties, the permeability would also increase, but that property was not measured. Progressive leaching by flowing water, which increases permeability, leads to self-accelerating attack; this mode of deterioration probably constitutes the greatest threat to cement in abandoned wells.

Far more serious than leaching by water is the reaction of CH with carbonic acid to create calcium bicarbonate, $Ca(HCO_3)_2$:

$$Ca(OH)_2 + 2H_2CO_3 \rightarrow Ca(HCO_3)_2 + 2H_2O \tag{4}$$

Calcium bicarbonate is two orders of magnitude more soluble than CH, as shown in Figure 9, and the solubility increases as the pressure of CO_2 rises, and the pH drops.

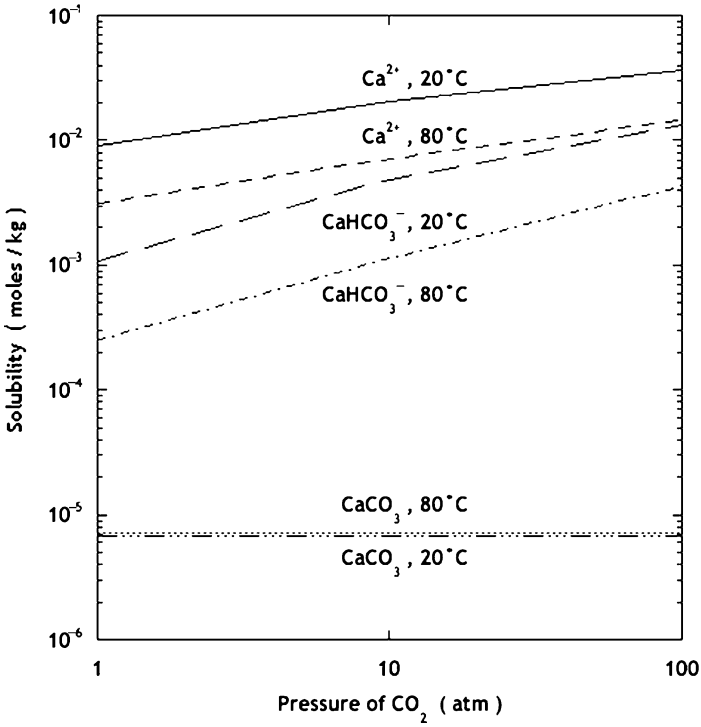

Figure 9: Solubility of the major species resulting from equilibration of water, CO_2, and limestone.

Although the carbonation of CH is favored, C-S-H can also be decomposed by carbonic acid. This reaction can be significantly accelerated by the increased porosity and permeability of the cement due to the absence of CH. The decomposition of C-S-H by H_2CO_3 can be approximated as [27]:

$$CaO{\cdot}SiO_2{\cdot}H_2O + H_2CO_3 \rightarrow Ca^{2+} + CO_3^{2-} + SiO_2{\cdot}H_2O \tag{5}$$

This produces soluble species and silica gel, which is highly porous and has very poor mechanical properties.

There are numerous studies in the literature on the degradation of cement in acidic water. Some have been on the degradation at elevated temperature and pressure, which is typically found in geothermal wells [28–34]. Others have been tested at atmospheric pressure and temperature but with varying pH [19,35–38]. Milestone et al. [31,32] investigated the failure of geothermal wells in the Broadlands, at temperatures of 150 and 250 °C. The primary focus was on the added silica, which, under ambient temperature and pressure, tends to drive down the permeability by reacting with the CH and creating more C-S-H. The hypothesis was that, since CH was depleted by the pozzolanic reaction of silica and CH, aggressive CO_2 immediately attacked the C-S-H, which accelerated the degradation process. Strength retrogression was observed, and the depth of carbonation increased with silica content to a maximum depth of 3 mm. The permeability decreased after exposure to carbonic acid, when the amount of added silica was less than 20%; however, as the amount of added silica exceeded 20%, the permeability increased by 50–3000% after only 2 weeks exposure to CO_2.

Bruckdorfer [29] varied the size (and thus the surface to volume ratio) of his samples and tested them after 3 and 6 weeks after exposure at 79.4 °C and 20.68 MPa. After 6 weeks of exposure, both Classes C and H cement exhibited 80% strength loss; by decreasing the w/c from 0.53 to 0.42, the strength loss was reduced by 25%.

Apparently the only study performed on cement recovered from a well was done by Shen and Pye [33], who obtained samples from the intermediate casing annulus, the production casing annulus, and the re-drilling casing annulus. Most samples had permeability below the API recommended value of 0.2 mD. Attempts to correlate permeability and strength with $C\bar{C}$ content and in-service time were unsuccessful. However, the cement started to lose strength and gain permeability after nine production shutdowns, an effect attributed to thermal stresses during the shutdowns. Fissures of 0.1–5 mm were observed extensively, and some of the finer fissures were filled with $C\bar{C}$, but it could not be determined whether these fissures were due to the coring process or the chemical attack.

Revertegat et al. [37] published a paper on the effect of pH on the durability of paste immersed in a bath of water. At a pH of 4.6, obtained by controlling the partial pressure of CO_2 over the bath, 70–75% decalcification of samples occurred after 3 years of exposure, leaving a weak and highly permeable gel of silica and alumina. Electron microprobe analysis revealed a sharp concentration gradient, indicating a deterioration front between the corroded and uncorroded regions. As the deterioration progressed, cracks large enough to be visible under optical microscopes were observed within the corroded region. The results from X-ray fluorescence showed that the decrease in CaO over 3 years obeyed Fick's Law, indicating diffusion-controlled deterioration.

These studies have yielded useful indications of the severity of attack to be expected under conditions of storage, but none have comprehensively looked at performance parameters, such as strength and permeability, along with microstructure and chemistry, such as the degree of hydration and crystal structure. There are no data available for transport rates in cement subjected to attack by carbonated brine, and essentially nothing is available within the temperature and pressure range of interest for CO_2 storage. Therefore, we are undertaking a comprehensive study of the mechanical and transport properties of cement subjected to the range of pH and temperature expected to exist in carbonated brine.

EXPERIMENTAL PROGRAM

As indicated in Figure 8, if injection is done at a depth of 1–2 km, the pH of the brine will fall in the range of 3 in purely quartzitic sandstone formations and 5 in limestone formations; assuming a temperature gradient of 30 °C/km, the temperature will be about 50–85 °C at that depth. Therefore, we are studying the durability of cement exposed to brine (3 wt% NaCl) in that range of pH and temperature. The samples are prepared from Class H cement (Lafarge; 61% C_3S, 16.3% C_2S, 16.6% C_4AF, 0 C_3A) with additions of 0, 6, or 12 wt% bentonite. The cement pastes are mixed at room temperature and cured in brine at 20, 50, or 85 °C for 28 days, prior to exposure to acidic brine. One set of samples consists of a cylinder of stone (5.5 cm diameter by 10 cm high) with a 2.5 cm hole drilled parallel to the axis, but off center, as shown in Figure 10. Cylinders have been prepared using Salem limestone (13.2% porosity, density 2.33 g/cm^3) and Berea sandstone (19.1% porosity, density 2.14 g/cm^3). The varying thickness of the stone results in a difference in

the time to transport acid to the cement, so that the depth of attack varies around the perimeter. The diffusion coefficient of water in the pores of the sandstone, measured using ^{1}H NMR, is $D = 6 \times 10^{-10}$ m^2/s (which is approximately four times slower than the self-diffusion coefficient in bulk water, owing to the tortuosity of the pore network). The time to diffuse a distance x is approximately $t = x^2/D$, and the thickness of the stone around the cement core is between 5 and 25 mm, so the diffusion time ranges from approximately 12 to 290 h. To investigate the effect of exposure to the acified brine, the cylinder is cut into slices approximately 1 cm thick and the faces are sealed between sheets of Teflon and stainless steel, so that the brine can only enter radially through the stone.

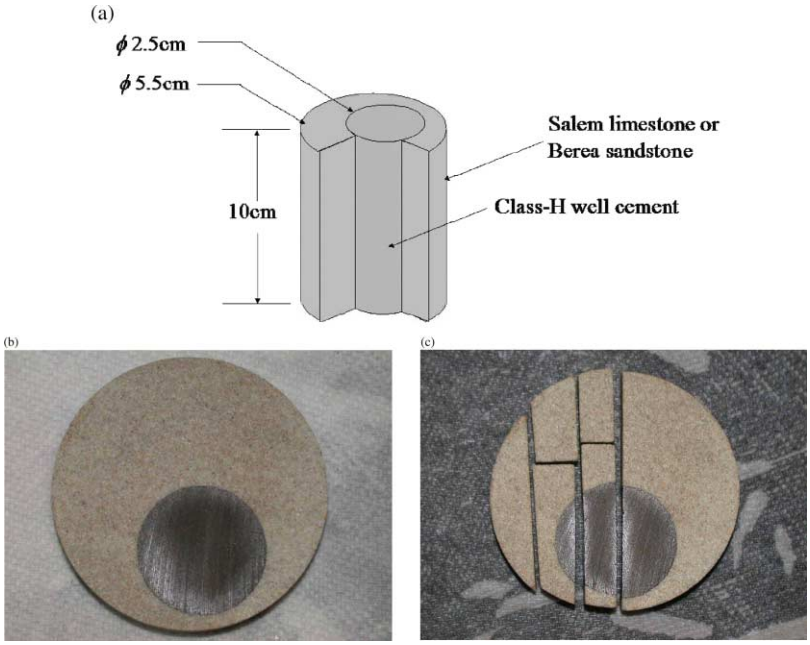

Figure 10: (a) Design of sample consisting of cylinder of stone with off-center hole parallel to the axis, filled with cement paste; (b) slice from cylinder is exposed to acidic brine, then cut into sections for analysis of structure, composition, and properties. From Ref. [45].

The slices are immersed in a static bath with a volume of brine about 35 times greater than that of the samples, at a temperature of 20, 50, or 85 °C. The pH is controlled by saturating the brine with carbon dioxide at ambient pressure, which produces pH 4, then adjusting with NaOH or HCl. If the formation used for storage is primarily quartzitic rock, there will be negligible dissolution of the stone in the brine. To simulate that situation, the samples made with the Berea sandstone are exposed to a brine containing 3% NaCl that is saturated with silica and CO_2 at atmospheric pressure; the pH is adjusted to 3, 4, or 5. On the other hand, if the formation is limestone, there will be substantial dissolution near the point of injection, so we expect that the brine will be saturated with the components of calcium carbonate by the time it reaches any cement-filled wells. Therefore, the samples made with Salem limestone are exposed to a brine saturated with calcium carbonate, with a pH of 4, 5, or 6.

At appropriate intervals of time (depending on temperature and pH), samples are removed for analysis. The slice is cut into several pieces, as shown in Figure 10b, and subjected to the following examinations: (a) the composition is profiled along the radius of the cement core using an electron microprobe; (b) the structure (porosity, mineral distribution, cracking) is examined using an environmental scanning electron

microscope (ESEM), which permits imaging without drying of the sample; (c) the hardness is profiled along the radius of the cement core using Vickers indentation, to reveal changes in mechanical integrity of the cement.

Another set of cement samples is cast in the form of cylinders with diameter of 8 or 12 mm and length of about 250 mm. This form is chosen to permit measurement of the permeability by the beam-bending method recently developed in this lab [39]. The saturated cylinder of cement paste is subjected to a sudden deflection in three-point bending, which causes compression of the sample above the midplane and tension below. The liquid in the pores in the upper half of the sample is compressed, while tension is created in the pores in the lower half, resulting in flow of the liquid within the cylinder to eliminate the gradient in pore pressure. The force required to sustain a constant deflection of the cylinder changes as the pore pressure equilibrates, and the rate of equilibration depends on the permeability, so the permeability of the sample can be found by analyzing the force exerted by the cylinder against the pushrod. This method has been applied to cement paste to determine the permeability of mature paste [40,41] and the evolution of permeability and viscoelastic properties in young paste [42]). A typical result is shown in Figure 11, for a sample of Class H cement prepared with a water/cement ratio of 0.38, then aged in 3% brine at neutral pH for 28 days at 50 °C. The permeability is found to be 7.4×10^{-20} m^2 (equivalent to 7.4×10^{-13} m/s); although the permeability is quite low, the measurement was completed in about 1 h.

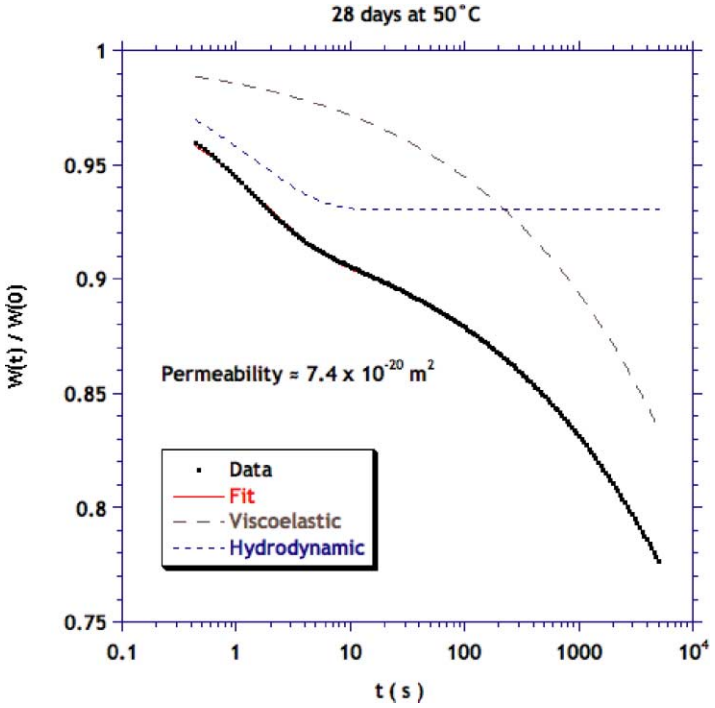

Figure 11: Normalized force, W, on saturated cylinder of Type H cement paste (water/cement ratio = 0.38, aged 28 days at 50 °C in 3% NaCl solution) versus time under load in three-point bending. The data are the symbols and the fit to the theoretical curve is invisible under the data points. The relaxation of the pore pressure is described by the Hydrodynamic relaxation curve (short dashes) and the viscoelastic stress relaxation is described by the Viscoelastic curve (long dashes); the total relaxation is the product of the two. The plateau in the Hydrodynamic curve occurs when the pore pressure reaches atmospheric pressure. Analysis of the kinetics of relaxation using the theory in Ref. [39] yields a permeability of 7.4×10^{-20} m^2.

Cylindrical samples of cement paste containing 0, 6, and 12% bentonite, with dimensions suitable for beam-bending, are exposed to flowing brine with pH values of 3 or 4 at temperatures of 20, 50, and 85 °C. The composition of the effluent is monitored using ICP analysis to determine the rate of attack on the cement. Samples are periodically removed from the bath and subjected to three-point bending to determine changes in permeability and viscoelastic properties. Small sections are then cut from the end of the rod for analysis of compositional and structural changes, using ESEM and microprobe.

These experiments on stone and cement are performed at ambient pressure, because we expect the chemical reactions to be strongly affected by temperature and pH, but weakly dependent on pressure [43,44]. To test this assumption, some experiments are performed at elevated pressure using apparatus developed by Bruant et al. [43]. Figure 12 shows an example of two samples of Class H cement paste that were exposed to brine under 10 MPa CO_2 at 50 °C for 9 days; one sample had been cured at 21 °C and the other at 50 °C for 3 months prior to exposure [45]). There is a reaction rim about 1 mm deep that has turned from gray to red, apparently owing to the change in oxidation state of the iron; within the reaction zone there are several rings with slightly different colors. The ESEM reveals that the structure of the outer layer is more porous, and chemical analysis by energy dispersive X-ray spectroscopy (EDX) reveals extensive removal of calcium. It is expected (e.g. Ref. [46]) that the acid will dissolve the CH in the paste, and then leach calcium from the C-S-H, and that process is evident in this sample. In the sample that had been cured at 50 °C, the Ca/Si ratio in the reacted zone is 1.25, whereas the ratio in the unreacted zone is about 3. The ratio would be about 1.7, if only C-S-H were present, so the leaching has decalcified the C-S-H, as well as removing the CH. Preliminary results indicate a similar depth of reaction in samples exposed to pH 2.7 at 53 °C at ambient pressure, but these comparisons must be extended to much longer times to confirm the influence of pressure.

MODELING OF ACID ATTACK

The rapid attack of the sample in Figure 12 is consistent with preliminary results of our experiments at ambient pressure. Clearly the potential risk to the cement in abandoned wells is great, so it is essential to know the composition of the solution that will come into contact with them. For this reason, detailed simulations of the composition and flow rate of the carbonated brine are in progress using Dynaflow [46], which is a finite element program capable of analyzing flow with proper coupling of pore pressure and strain in the formation. The partitioning of CO_2 and H_2O between liquid and vapor species is achieved in a "flash calculation" based on a new approach [47]) that is faster than the Peng–Robinson [48] approach, and is consistent with the solubility data of Duan and Sun [49]. Equilibrium requires that the fugacity of a component be the same in each phase. For two components in two phases, the two fugacity equations alone determine the two independent phase mole fractions. This separation of partitioning and equilibrium calculations is not possible for CO_2 brine flash calculations, where the brine's salinity has a strong effect on solubility of CO_2, and the salinity depends on the water and salt availability. We use fugacity expressions that provide the equilibrium equations for the complete salinity range with a single fit to CO_2 solubility in brine at one temperature and pressure. The expressions are simple enough to allow a new fit for each flash calculation. The calculation predicts the concentration of water in the vapor and the concentrations of salt and CO_2 in the liquid. It also precipitates salt when the water-rich phase is supersaturated with salt by evaporation of water into the vapor phase, and dissolves solid salt into an undersaturated liquid phase. Finally, the flash calculation indicates no-vapor and no-liquid conditions along with any partitioning with precipitated salt. Figure 13 shows how well the calculation matches the data of Duan and Sun for the solubility of CO_2 in saline water.

Figure 14 shows the results of a simulation of injection of CO_2 at a rate of 100 kg/s (3 megatons/yr) into a formation at a pressure of 10 MPa at temperature 60 °C, corresponding to a depth of about 1 km; the formation is assumed to have a permeability of 10^{-13} m^2 (100 mD) and porosity of 10%. The total dissolved solids in the brine is assumed to be 5 wt%. The saturation of supercritical fluid is near unity at the injection site, but drops rapidly with distance; the advancing front has a vapor saturation that ranges from about 25 to 0% over a distance of about 75 m. The liquid saturation rapidly drops near the site of injection, reaching zero in about 2.5 years, at which point the leading edge of the plume has advanced approximately 1200 m; thereafter, the profile becomes self-similar, so that it is a function only of the Boltzmann variable, $R/\sqrt{t}$, where R is the distance from the injection site and t the time. This profile, which is shown in Figure 15, can be used to determine the size of the plume at any subsequent time or position surrounding the injection site.

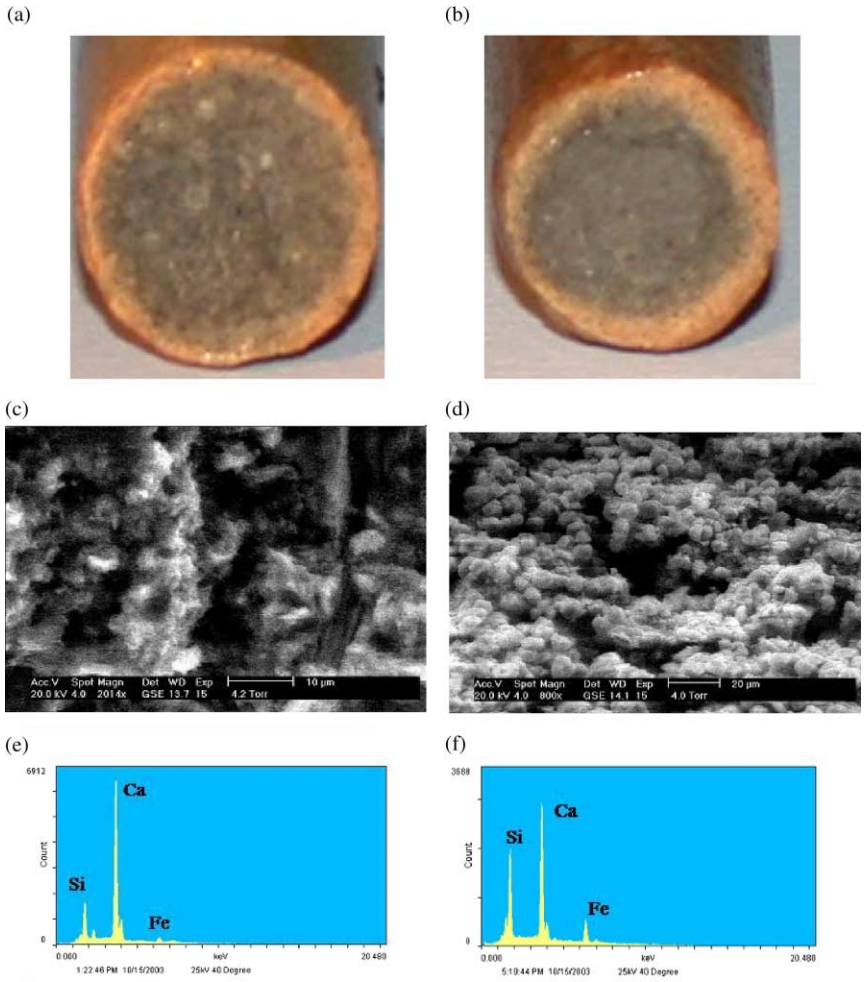

Figure 12: The effect of CO_2-rich water at 10 MPa and 50 °C for 9 days on cement paste samples. (a) Reaction rims on a cement sample cured at 23 °C prior to CO_2 exposure. (b) Reaction rims/color change on a cement sample cured at 50 °C prior to CO_2 exposure. (c) ESEM micrograph of the middle part of cement sample, with a typical open texture CSH due to curing at 50 °C. (d) ESEM micrograph of cement paste subjected to high pressure carbonation, (e) and (f) show EDX composition of cement paste prior and after CO_2 exposure showing a Ca depletion due to the carbonic acid attack, observed as different Si/Ca ratios. From Ref. [45].

To get an idea of the duration of exposure of a well to acid, we multiply the flux of liquid by the mole fraction of dissolved CO_2 in the brine, with the result shown in Figure 16. This plot indicates that a well located approximately 800 m from the injection site would be exposed to the acidified brine after about a year. The peak of the acid flux corresponds to the edge of the plume, where the liquid saturation is high ($>75\%$) and the liquid is saturated with CO_2. At the peak, the flux of aqueous carbonate species is roughly 100 kg/m^2 yr for a period of about a month, then drops to approximately 10 kg/m^2 yr for approximately 10 years. Therefore, as the carbonated brine passes by an abandoned well, the cement will suffer the most

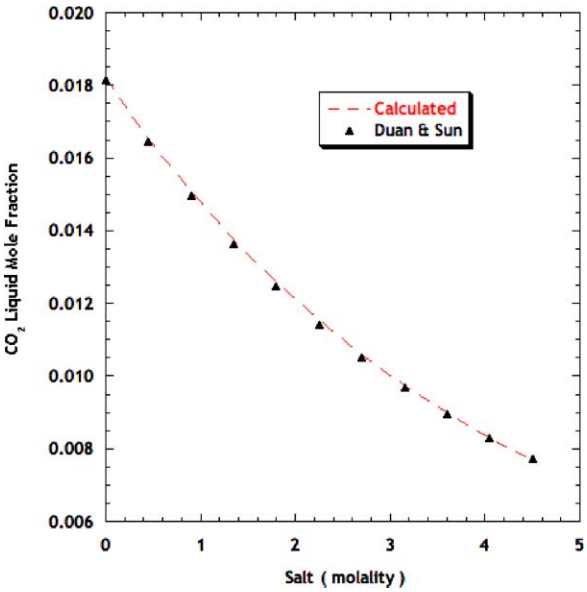

Figure 13: Flash calculation of mass fraction of (a) CO_2 dissolved in liquid phase, along with data of Duan and Sun [49] and (b) water in vapor phase, as functions of salt content.

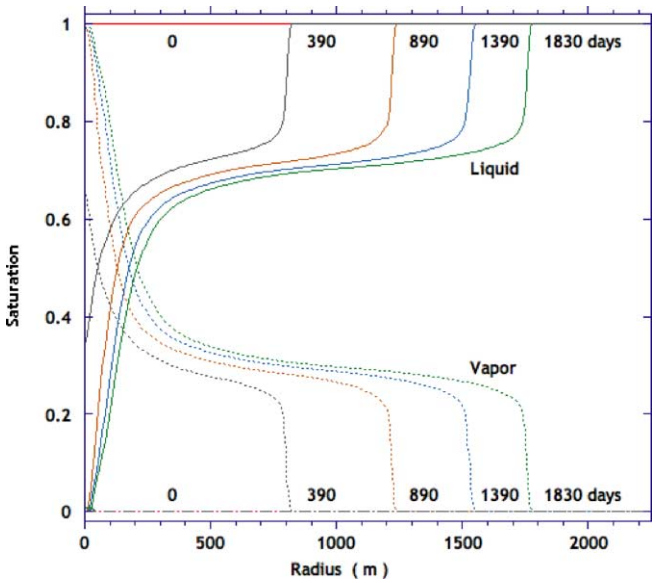

Figure 14: Calculated saturation profiles for liquid and vapor phases during injection of CO_2 at a rate of 100 kg/s (3 megatons/yr) into a formation at a pressure of 10 MPa at temperature 60 °C; the formation is assumed to have a permeability of 10^{-13} m^2 (100 mD) and porosity of 10%. The total dissolved solids in the brine is assumed to be 5 wt%.

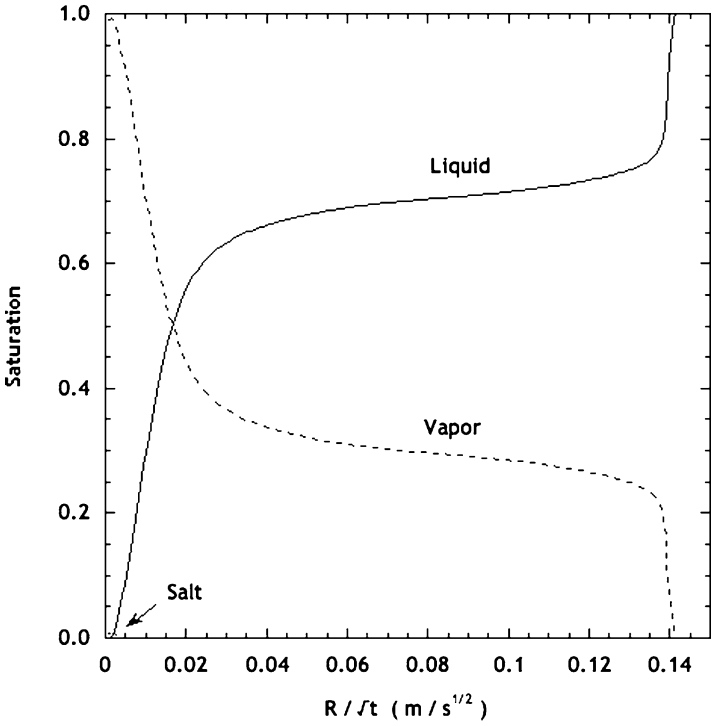

Figure 15: Saturation of pore space with liquid and vapor phases as a function of radial distance from the injection site (*R*) divided by the square root of time; these curves apply from the time when the liquid saturation near the injection site drops to zero (viz., ~900 days, under the conditions of this simulation, which are the same as in Figure 14).

aggressive attack over a period of a few months, but will continue to be exposed to a flow of acidic brine for a decade (under the conditions of this simulation).

The corrosion experiments will provide quantitative information about the depth of attack that could occur during that period. The greatest risk of leakage would occur if there were an annular gap between the cement and the cap rock, or a region of permeable cracks from drilling damage near the well, as shown in Figure 2. In that case, the acidified brine would flow through the annulus for a period of months or years, and could turn a small leak into a large one by dissolving the cement. The kinetics of this process will be explored by simulating flow through an annulus using Dynaflow, together with experimental data on the corrosion rate of cement.

CONCLUSIONS

The potential leakage of CO_2 from a geological storage site through existing wells represents a major concern. An analysis of well distribution in the Viking Formation in the Alberta basin, a mature sedimentary basin representative for North American basins, shows that a CO_2 plume and/or acidified brine may encounter up to several hundred wells. If carbon dioxide is geologically stored in regions, such as this, that have experienced intensive exploration for petroleum products, the acidified brine will come into contact with numerous abandoned wells. Corrosion of the cement that seals the well could lead to rapid leakage, so

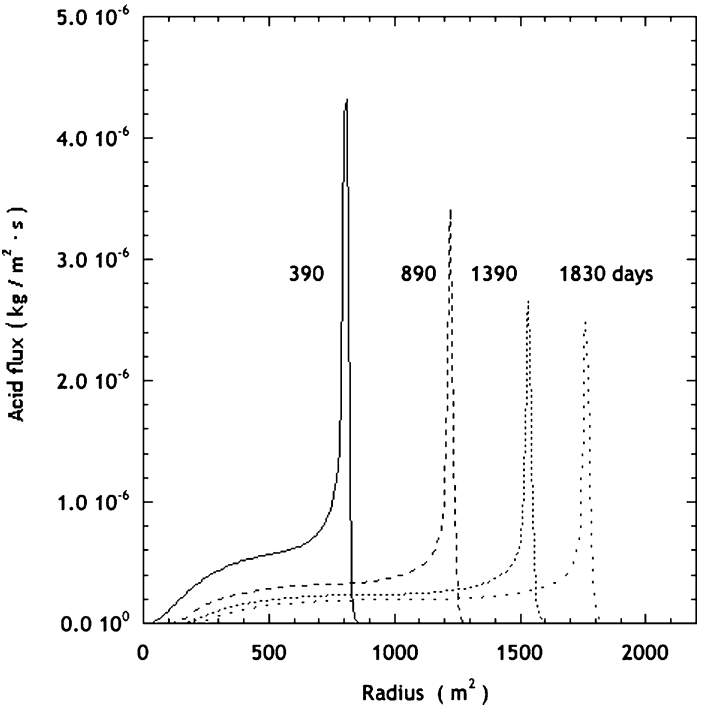

Figure 16: Flux of aqueous carbon species, under the conditions specified in Figure 14. The acidic brine would reach a well 800 m from the injection site in about 1 year; the edge of the plume has a high saturation and acid concentration, but it passes quickly. The acid flux continues for years at a lower intensity (owing to reduced saturation of the pore space with liquid) as the plume expands.

it is essential to determine the duration and intensity of exposure to the acid. Detailed numerical simulations with Dynaflow, incorporating a flash calculation to find the phase distribution and speciation in the brine, indicate that the carbonated brine may spend years in contact with the cement in abandoned wells. Preliminary results from an ongoing experimental study of cement corrosion indicate that the rate of attack is rapid, when the pH of the solution is low, so the risk of leakage will be high if the acidic brine can flow through an annulus and bring fresh acid into contact with the cement.

ACKNOWLEDGEMENTS

This work was supported by BP and Ford Motor Company through the Carbon Mitigation Initiative at Princeton University.

REFERENCES

1. Railroad Commission of Texas, Current and historical oil and gas wells and other existing wells, 1999, http://www.rrc.state.tx.us/index.html.
2. S.E. Gasda, S. Bachu, M.A. Celia, Spatial characterization of the location of potentially leaky wells penetrating a geological formation in a mature sedimentary basin, *Environ. Geol.* (2004) in press.
3. E.B. Nelson, *Well Cementing*, Schlumberger Educational Services, Sugar Land, TX, 1990.
4. S.E. Gasda, CO_2 sequestration into a mature sedimentary basin: determining the capacity and leakage potential of a saline aquifer formation, Master's Thesis, Princeton University, 2004.

5. J.M. Nordbotten, M.A. Celia, S. Bachu, Analytical solutions for leakage rates through abandoned wells, *Water Resour. Res.* **40** (2004) W04204, doi 10.1029/2003WR002997.
6. J. Nordbotten, M.A. Celia, S. Bachu, H.K. Dahle, Analytical solution for CO_2 leakage between two aquifers through an abandoned well, *Environ. Sci. Technol.* (2004) in press.
7. S.E. Gasda, M.A. Celia, Upscaling relative permeabilities in a structured porous medium, in: C.T. Miller, M.W. Farthing, W.G. Gray, G.F. Pinder (Eds.), *Proc. XVth CMWR Conf.*, 13–17 June 2004, Chapel Hill, NC, New York: Elsevier (2004) pp. 793–804.
8. A.S. Altevogt, M.A. Celia, Numerical modeling of carbon dioxide in unsaturated soils due to deep subsurface leakage, *Water Resour. Res.* **40** (2004) W03509: doi: 10.1029/2003WR00284.
9. A.S. Altevogt, P.R. Jaffe, Modeling the effects of gas-phase CO_2 intrusion on the biogeochemistry of variably saturated soils, in: C.T. Miller, M.W. Farthing, W.G. Gray, G.F. Pinder (Eds.), *Proc. XVth CMWR Conf.*, 13–17 June 2004, Chapel Hill, NC, New York: Elsevier (2004) 817–826.
10. S. Wang, P.R. Jaffe, Dissolution of trace metals in potable aquifers due to CO_2 release from deep formations, *Energy Convers. Manage.* **45** (18–19) (2004), 2833–2848.
11. S. Bachu, J.M. Nordbotten, M.A. Celia, Evaluation of the spread of acid gas plumes injected in deep saline aquifers in western Canada as an analogue for CO2 injection in continental sedimentary basins, *Proceedings, Seventh International Greenhouse Gas Technologies Conference,* Vancouver, BC, September 5–9, 2004.
12. E. Lindeberg, Escape of CO_2 from aquifers, *Energy Convers. Manage.* **38S** (1997) S235–S240.
13. T.F. Xu, J.A. Apps, K. Pruess, Reactive geochemical transport simulation to study mineral trapping for CO_2 disposal in arenaceous formations, *J. Geophys. Res. Solid Earth* **10** (B2) (2003) 2071.
14. J.M. Nordbotten, M.A. Celia, S. Bachu, Injection and storage of CO_2 in deep saline aquifers: analytical solution for CO_2 plume evolution during injection, *Transport Porous Media* (2004) in Press.
15. A.M. Neville, *Properties of Concrete*, fourth ed., Wiley, New York, NY, 1997.
16. H.F.W. Taylor, *Cement Chemistry*, second ed., Thomas Telford, London, 1997.
17. H. Jennings, Colloid model of C-S-H and implications to the problem of creep and shrinkage, *Mater. Struct. Concr. Sci. Eng.* **37** (2004) 59–70.
18. T. Hartmann, P. Paviet-Hartmann, J.B. Rubin, M.R. Fitzsimmons, K.E. Sickafus, The effect of supercritical carbon dioxide treatment on the leachability and structure of cemented radioactive waste-forms, *Waste Manage.* **19** (1999) 355–361.
19. A. Hidalgo, C. Andrade, C. Alonso, Role of alkaline reserve in the acidic resistance of cement pastes, in: J. Skalny, J. Gebauer, I. Odler (Eds.), *Material Science of Concrete: Calcium Hydroxide in Concrete*, The American Ceramic Society, Westerville, OH, 2001, pp. 93–111.
20. T.C. Powers, L.E. Copeland, H.M. Mann, Capillary continuity or discontinuity in cement pastes, *J. Portland Cem. Assoc. Res. Dev. Lab.* (1959) 38–48. May.
21. F. Adenot, M. Buil, Modelling of the corrosion of the cement Paste by deionized water, *Cem. Concr. Res.* **22** (2/3) (1992) 489–496.
22. D.P. Bentz, E.J. Garboczi, Modeling the leaching of calcium hydroxide from cement paste: effects on pore space percolation and diffusivity, *Mater. Struct.* **25** (1992) 523–533.
23. C. Carde, R. Crancois, J.-P. Ollivier, Microstructural changes and mechanical effects due to the leaching of calcium hydroxide from cement paste, in: K.L. Scrivener, J.F. Young (Eds.), *Mechanisms of Chemical Degradation of Cement-Based Systems*, E&FN Spon, London, England, 1997, pp. 30–37.
24. B. Delagrave, J. Gerard, Marchand, Modelling the calcium leaching mechanisms in hydrated cement pastes, in: K.L. Scrivener, J.F. Young (Eds.), *Mechanisms of Chemical Degradation of Cement-Based Systems*, E&FN Spon, London, England, 1997, pp. 38–49.
25. B. Kienzler, P. Vejmelka, H.-J. Herbert, H. Meyer, C. Altenhein-Haese, Long-term leaching experiments of full-scale cemented waste forms: experiments and modeling, *Nucl. Technol.* **129** (1) (2000) 101–118.
26. J. Marchand, D. Bentz, E. Samson, Y. Maltais, Influence of calcium hydroxide dissolution on the transport properties of hydrated cement systems, in: J. Skalny, J. Gebauer, I. Odler (Eds.), *Material Science of Concrete: Calcium Hydroxide in Concrete*, American Ceramic Society, Westerville, OH, 2001, pp. 113–129.
27. J. Cowie, F.P. Glasser, The reaction between cement and natural waters containing dissolved carbon dioxide, *Adv. Cem. Res.* **4** (15) (1991) 119–134.
28. D.D. Onan, Effects of supercritical carbon dioxide on well cements, *SPE Technical Paper No. 12593*, Society of petroleum Engineers, Richardson, TX, 1984, pp. 161–172.

29. R.A. Bruckdorfer, Carbon dioxide corrosion in oilwell cements, *SPE Technical Paper No. 15176*, Society of Petroleum Engineers, Richardson, TX, 1986, pp. 531–539.
30. N.B. Milestone, D.A. St John, J.H. Abbott, L.P. Aldridge, CO_2 corrosion of geothermal cement grouts, *Proceedings from the Eighth International Congress on the Chemistry of Cement in Rio de Janeiro,* Brazil, September, 1986, pp. 141–144.
31. N.B. Milestone, T. Sugama, L.E. Kukacka, N. Carciello, Carbonation of geothermal grouts—part 1: CO_2 attack at 150 °C, *Cem. Concr. Res.* **16** (6) (1986) 941–950.
32. N.B. Milestone, T. Sugama, L.E. Kukacka, N. Carciello, Carbonation of geothermal grouts—part 2: CO_2 attack at 250 °C, *Cem. Concr. Res.* **17** (1) (1987) 37–46.
33. J.C. Shen, D.S. Pye, Effects of CO_2 attack on cement in high-temperature applications, *SPE Technical Paper No. 18618*, Society of Petroleum Engineers, Richardson, TX, 1989, pp. 19–28.
34. J.W. Hedenquist, M.K. Stewart, Natural CO_2-rich steam-heated waters in the Broadlands–Ohaaki Geothermal System, New Zealand: their chemistry, distribution and corrosive nature, Transactions from the geothermal resources council, vol. 9, 1985, Part II, August, pp. 245–250.
35. J. Jambor, V. Zivica, Porosity of mortar and its influence on resistance against corrosion caused by aggressive carbon dioxide, *Proceedings from RILEM/IUPAC International Symposium on Pore Structure and Properties of Materials,* Prague, September 18–21, 1973, pp. F83–F93..
36. Y. Ballim, M.G. Alexander, Carbonic acid water attach of Portland cement based matrices, in: R.K. Dhir, J.W. Green (Eds.), *Proceedings from the International Conference on the Protection of Concrete*, September 11–12, 1990, pp. 93–104.
37. E. Revertegat, C. Richet, P. Gegout, Effect of pH on the durability of cement pastes, *Cem. Concr. Res.* **22** (1992) 259–272.
38. V. Zivica, A. Bajza, Acidic attack of cement-based materials—a review: part 2. Factors of rate of acidic attack and protective measures, *Construction Building Mater.* **16** (2002) 215–222.
39. G.W. Scherer, Measuring permeability of rigid materials by a beam-bending method: I. theory, *J. Am. Ceram. Soc.* **83** (9) (2000) 2231–2239.
40. W. Vichit-Vadakan, G.W. Scherer, Measuring permeability of rigid materials by a beam-bending method: III. Cement paste, *J. Am. Ceram. Soc.* **85** (6) (2002) 1537–1544.
41. J.J. Valenza II, G.W. Scherer, Measuring permeability of rigid materials by a beam-bending method: V. Cement paste plates, *J. Am. Ceram. Soc.* (2004) in press.
42. W. Vichit-Vadakan, G.W. Scherer, Measuring permeability and stress relaxation of young cement paste by beam-bending, *Cem. Concr. Res.* **33** (2003) (2003) 1925–1932.
43. D.E. Giammar, R.G. Bruant Jr., C.A. Peters, Forsterite dissolution and magnesite precipitation at conditions relevant for deep saline aquifer storage and sequestration of carbon dioxide, *Chemical Geology*, in press.
44. Y. Soong, A.L. Goodman, J.R. McCarthy-Jones, J.P. Baltrus, Experimental and simulation studies on mineral trapping of CO2 with brine, *Energy Convers. Manage.* **45** (2004) 1845–1859.
45. A. Duguid, R. Bruant, M. Radonjic, G.W. Scherer, M.A. Celia, C. Christopher, The effect of sequestered CO_2 on well cement, presented at Water–Rock Interactions Induced by Reservoir Exploration, CO_2 Sequestration, and Other Geological Storage, Paris, France, November 18–20, 2003.
46. J.-H. Prévost, DYNAFLOW: A Nonlinear Transient Finite Element Analysis Program, Princeton University, Princeton, New Jersey, NJ, 2003, last revision (2004).
47. R. Fuller, J. Prévost, A new approach to flash calculation and its implementation for three phase carbon dioxide, water, and salt mixtures, to be submitted.
48. D.-Y. Peng, D.B. Robinson, A new two constant equation of state, *Ind. Eng. Chem. Fundam.* **15** (1) (1976) 59–64.
49. Z. Duan, R. Sun, An improved model calculating CO_2 solubility in pure water and aqueous NaCl solutions from 273 to 533 K and from 0 to 2000 bar, *Chem. Geol.* **193** (2003) 257–271.